A synthesis of the Dibble et al. controlled experiments into the mechanics of lithic production

Supplementary Information 2

Li Li[1,*] Sam C. Lin[2,3] Shannon P. McPherron[1] Aylar Abdolahzadeh[4] Annie Chan[5,6] Tamara Dogandžić[7] Radu Iovita[8,9] George M. Leader[4,10] Matthew Magnani[11] Zeljko Rezek[12] Harold L. Dibble

∗ Corresponding author, li.li@eva.mpg.de

1. Department of Human Evolution, Max Planck Institute for Evolutionary Anthropology, Leipzig, Germany
2. Centre for Archaeological Science, School of Earth, Atmospheric and Life Sciences, University of Wollongong, Wollongong, New South Wales, Australia
3. Australian Research Council Centre of Excellence for Australian Biodiversity and Heritage, University of Wollongong, Wollongong, New South Wales, Australia
4. Department of Anthropology, University of Pennsylvania, Philadelphia, Pennsylvania, United States of America
5. Department of Asian Studies, Ludwig-Maximilians-Universität München, Munich, Germany
6. Centre de Recherche sur les Civilisations de l'Asie Orientale, Paris, France
7. MONREPOS Archaeological Research Centre and Museum for Human Behavioural Evolution, Neuwied, Germany
8. Center for the Study of Human Origins, Department of Anthropology, New York University, New York City, New York, United States of America
9. Early Prehistory and Quaternary Ecology, Department of Geosciences, Eberhard Karls University of Tübingen, Tübingen, Germany
10. Department of Sociology and Anthropology, The College of New Jersey, Ewing, New Jersey, United States of America
11. Department of Anthropology, University of Maine, Orono, Maine, United States of America
12. Department of Paleoanthropology, Collège de France, Paris, France

1 Introduction

With this synthesis paper, we are sharing the data produced by the Dibble and colleague experiments. This goal turned out to be a bit more difficult to realize than we had imagined. The database from the experiments was maintained over the years by Dibble. On his passing, we obtained a copy of the database, which includes a lot of cases (flakes and cores) and variables that were never used in the papers published by Dibble and colleagues for various reasons. As for the cases, for instance, some experiments did not work properly or some flakes represented only tests of the experimental setup. As for the unpublished variables, again, some of these measures just did not yield interesting results. The main complication is that there was not a list of which cases were used in which papers, and as the experiments continued, some cases were naturally used in multiple papers.

Our approach to solving this problem was to filter the database based on our collective knowledge of the experiments and their results, and then one of us (LL with some help from SPM) wrote this rMarkdown file to replicate the figures and main results of each of the experimental papers. When we compare the results presented here with the published papers, we find individual differences, but the overall pattern is the same. In other words, we cannot be sure to have included exactly the same set of cases in each instance, but our results are in line with the previously published results.

The data set used in our paper is then the same data set presented here. We have included the rMarkdown files so that others can see how we filtered the data to reproduce the results of each paper. Note that the figure and table numbers in what follows correspond to the figure and table numbers of the referenced paper.

2 Dibble & Rezek (2009)

2.1 The effect of PD and EPA

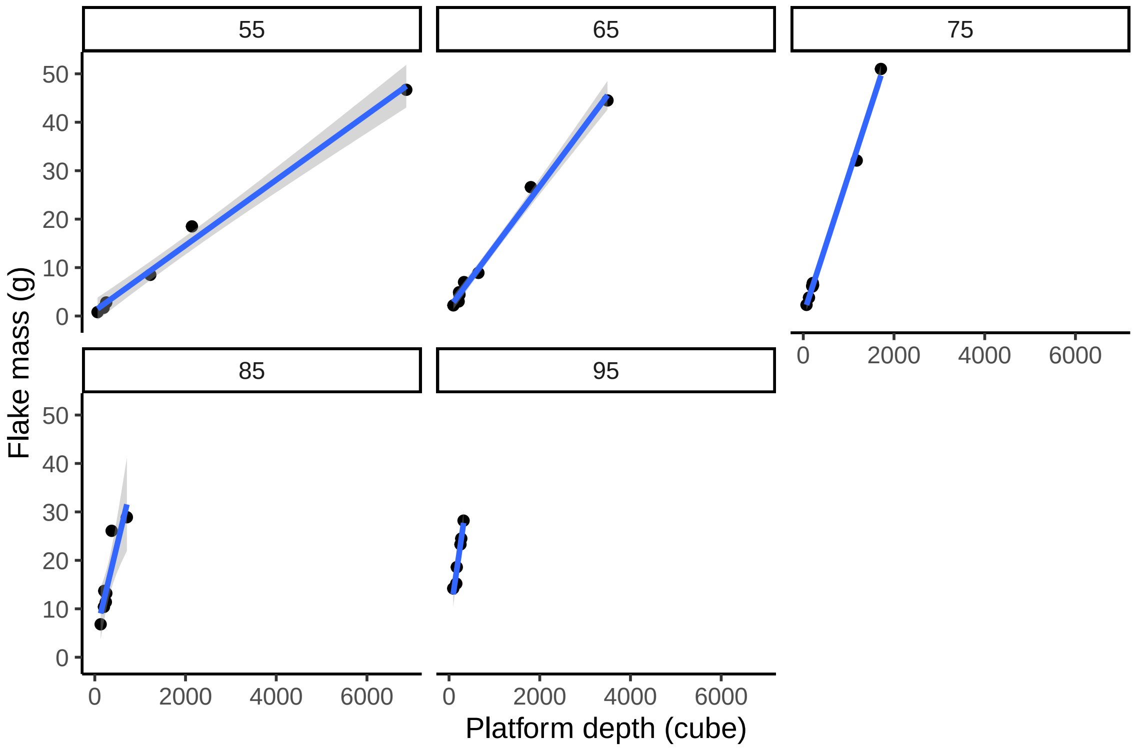

Fig. 6 Relationship between flake mass and PD (cubed).

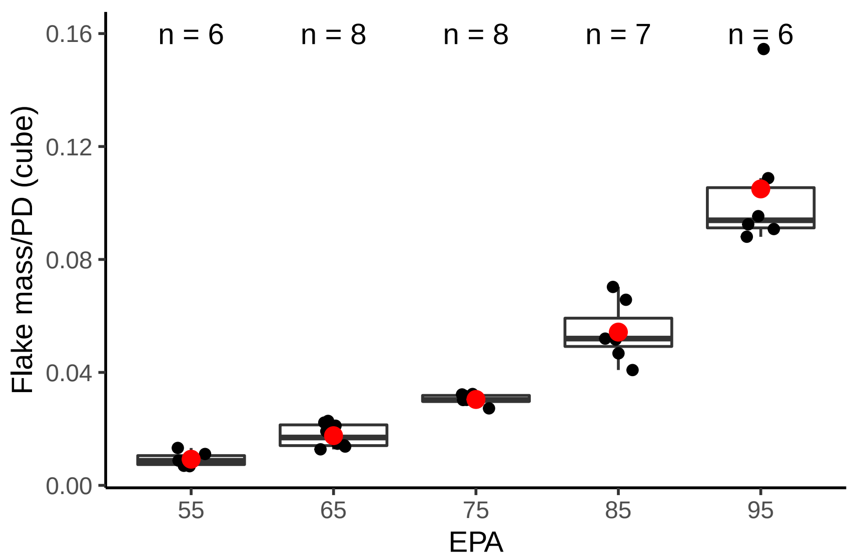

Fig.7 Box plot showing relationship between flake mass standardized by PD (cubed) and EPA.

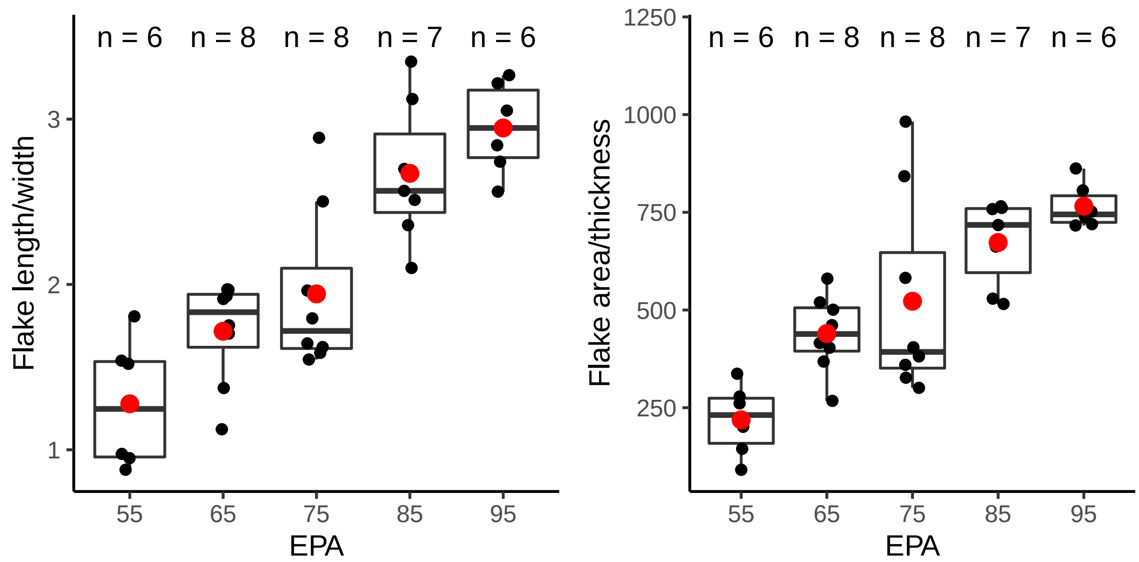

Fig.8 Boxplot showing changes in flake shape (left: length to width, right: area to thickness) as affected by different values of EPA.

2.2 The effect of AOB

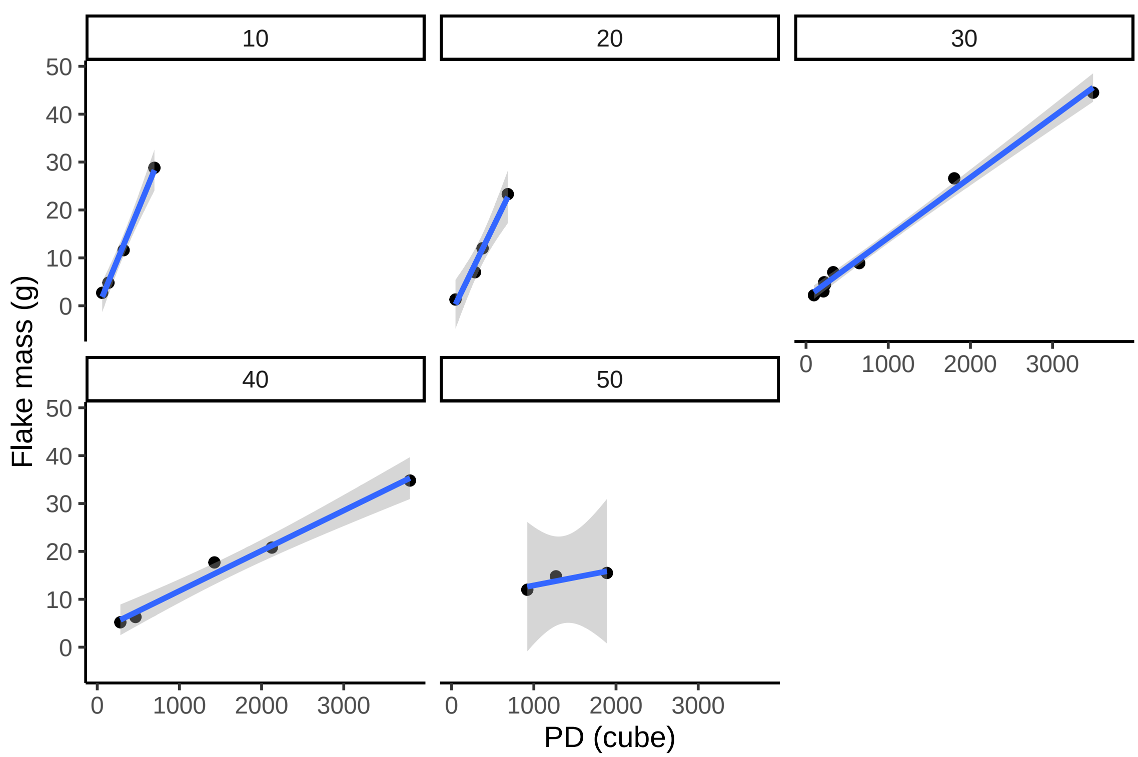

Fig.9 Relationship between flake mass and PD (cubed) for different AOBs.

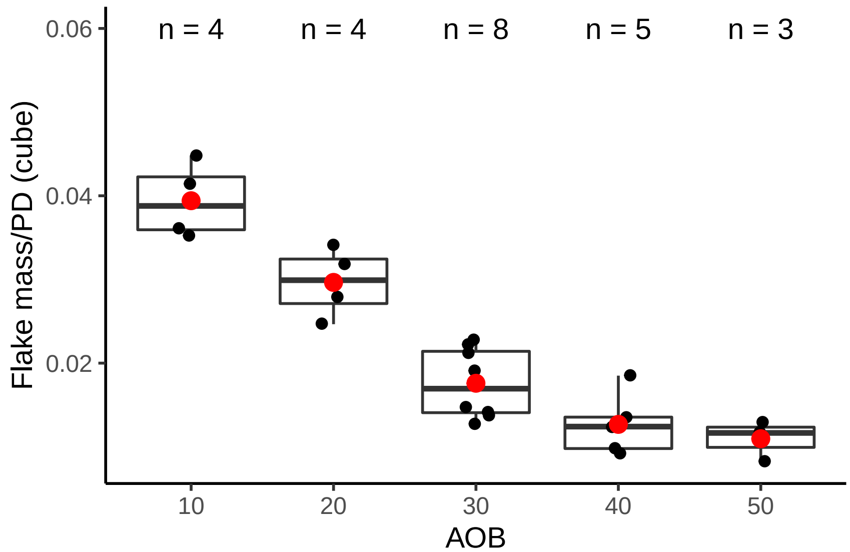

Fig.10 Boxplot showing relationship between flake mass standardized by PD (cubed) for different AOBs.

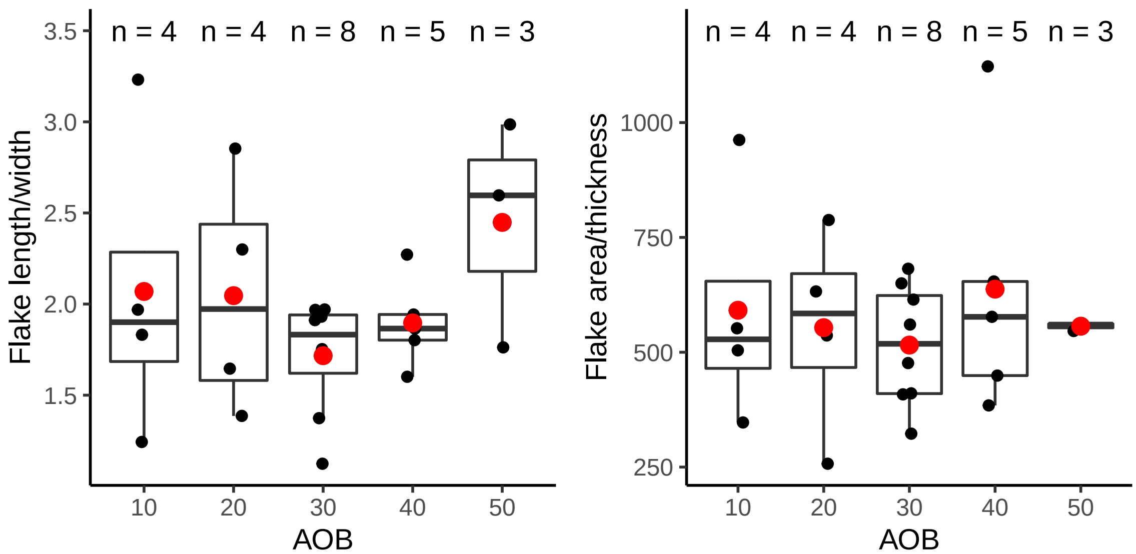

Fig.11 Boxplot showing changes in flake shape (left: length to width, right: area to thickness) as affected by different AOBs.

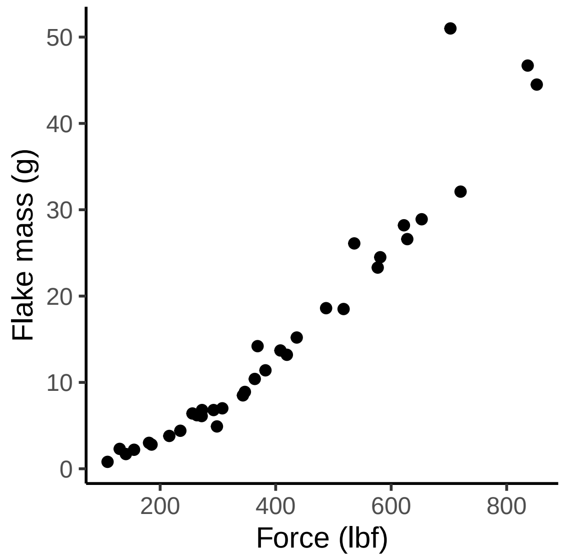

Fig.13 Flake mass as a function of force.

3 Rezek et al. (2011)

Table 1. dataset overview Breakdown of the number of flakes by core morphology and EPA.

Core type	55	65	75
SEMISPHERICAL	7	4	7
CENTERRIDGE	4	8	6
CONVERGENT	12	3	7
DIVERGENT	5	5	6
PARALLEL	5	8	6

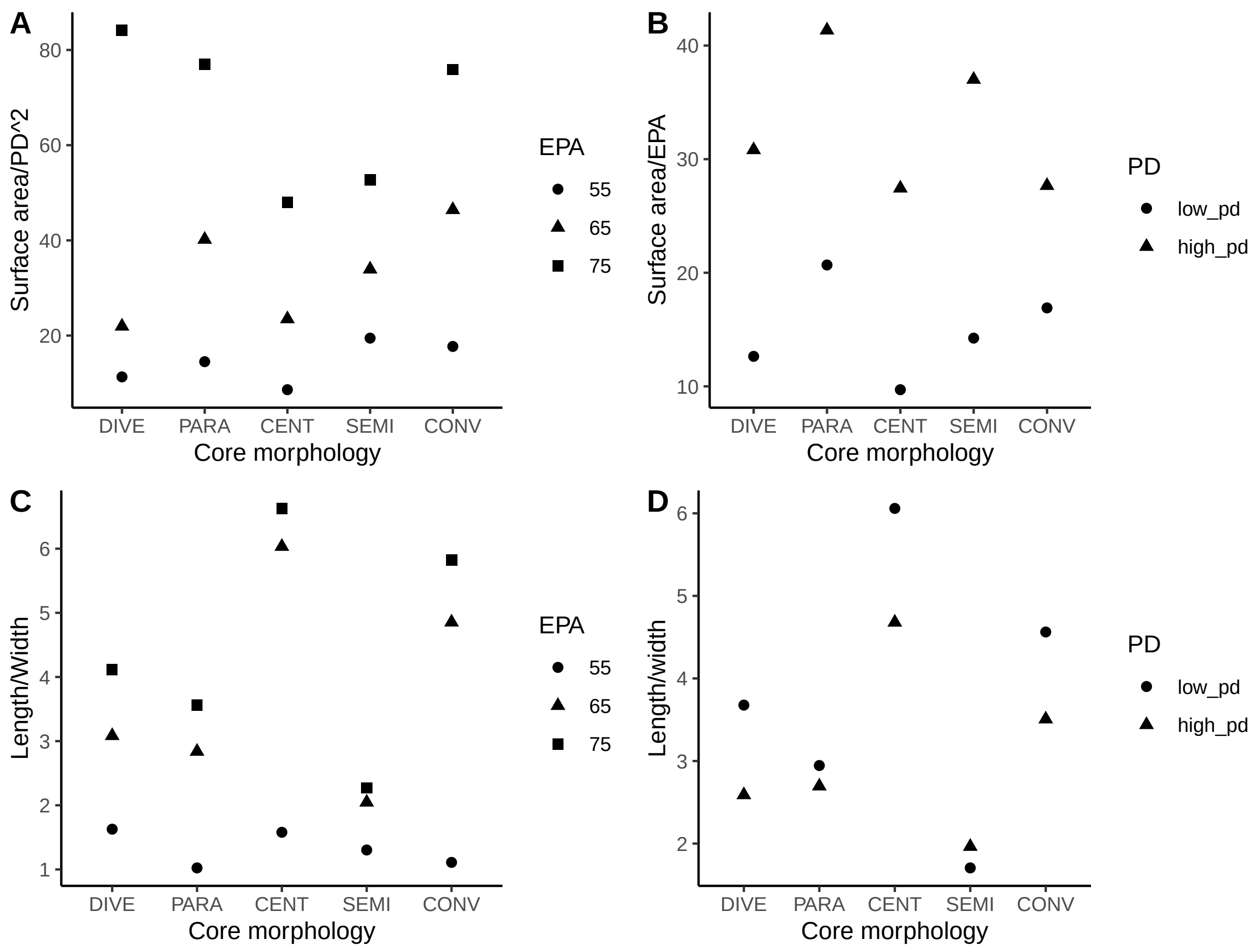

Fig.2 Graphs of both intra- and inter-Core variability on flake surface area, either controlling for PD (graph A) or EPA (graph B) and length/width (graphs C and D).

4 Magnani et al. (2014)

Table 1 Presence or absence of lipping by hammer material. Includes EPA = 55, 65, and 75, all values of AOB, and both locations of force (strikes both on the platform surface and the exterior edge of the platform).

Hammer material	Lipped	Not lipped	% Lipped
BONE50	50	1	98.04%
COPPER	35	27	56.45%
STEEL	20	39	33.90%

Table 2 Presence or absence of lipping by EPA, including flakes struck with both copper and steel hammers, both force locations, and a full range of AOBs. The lack of association with EPA holds even if AOB or location of force is controlled.

EPA	Lipped	Not lipped	% Lipped
55	4	1	80.00%
65	37	49	43.02%
75	14	16	46.67%

Table 3 Presence or absence of lipping by location of force. All flakes were produced with the copper hammer, EPA = 65, a full range of AOBs are included.

Force type	Lipped	Not lipped	% Lipped
Platform surface	5	11	31.25%
Exterior platform edge	20	13	60.61%

Table 4 Presence or absence of lipping by AOB. All flakes were produced with copper hammer and EPA = 65. Flakes produced by both locations of force (on edge or on platform) are included.

AOB	Lipped	Not lipped	% Lipped
Negative AOB	20	6	76.92%
Positive AOB	5	18	21.74%

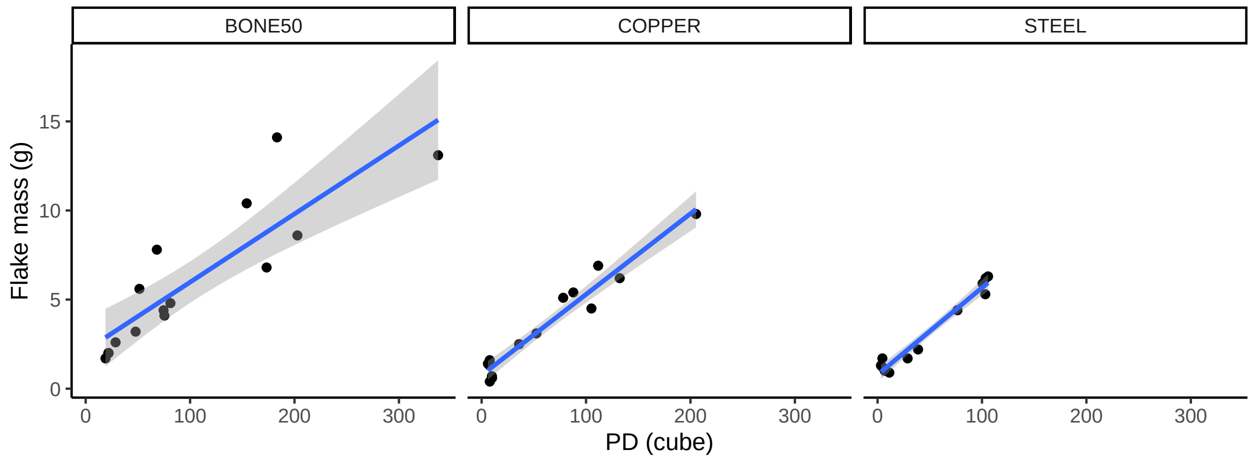

Fig.3 Scatter diagrams and correlations between flake weight and platform depth cubed by hammer material (EPA = 65, AOB = 5, both platform surface-struck and edge-struck flakes are included).

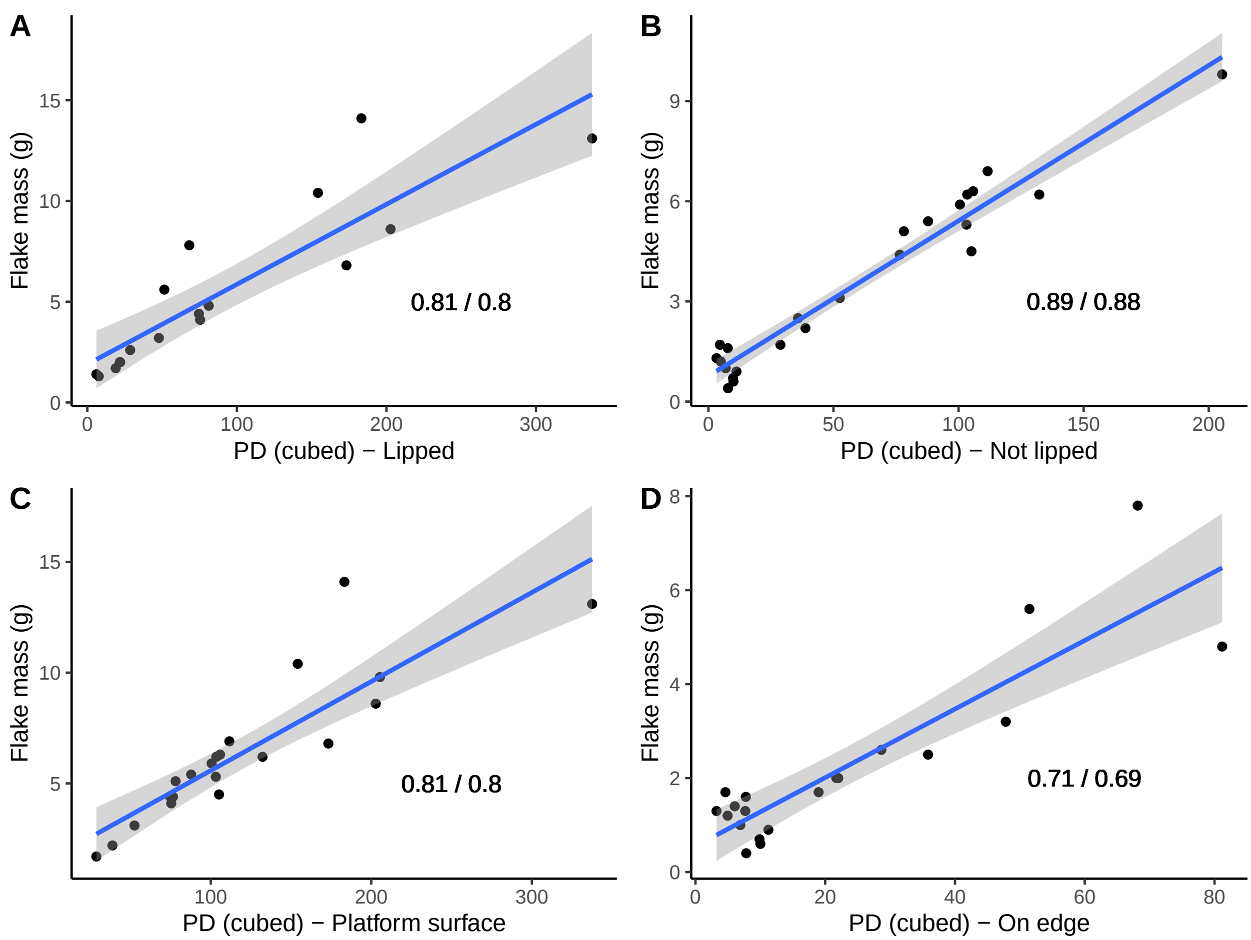

Fig.4 Correlations between flake weight and platform depth cubed for lipped and unlipped flakes, both platform-struck and edge-struck flakes are included. AOB = 5, EPA = 65, R^2 and adjusted R^2 are displayed on each plot.

Table 6 Relationship between location of force and the ratio of platform area to flake area, broken down by the presence or absence of lipping (EPA = 65, AOB = 5, all hammer types included).

Lipping	Force type	Mean	Count	SD
NO	Platform surface	0.034	6	0.008
NO	Exterior platform edge	0.010	4	0.006
YES	Platform surface	0.027	3	0.006
YES	Exterior platform edge	0.014	4	0.003

The ANOVA test results show that the differences in platform area to flake area between the two different strike locations are significant for both lipped and unlipped flakes.

For flakes with lipped platforms, the difference between the ratio of platform area and flake surface area is significant between the locations of force:

```
            Df    Sum Sq   Mean Sq F value Pr(>F)
forcetype    1 0.0003181 0.0003181   13.74 0.0139 *
Residuals    5 0.0001158 0.0000232
---
Signif. codes:  0 '***' 0.001 '**' 0.01 '*' 0.05 '.' 0.1 ' ' 1
```

For flakes with unlipped platforms, the difference between the ratio of platform area and flake surface area is also significant between the locations of force:

```
            Df    Sum Sq  Mean Sq F value   Pr(>F)
forcetype    1 0.0013901 1.39e-03   26.36 0.000891 ***
Residuals    8 0.0004219 5.27e-05
---
Signif. codes:  0 '***' 0.001 '**' 0.01 '*' 0.05 '.' 0.1 ' ' 1
```

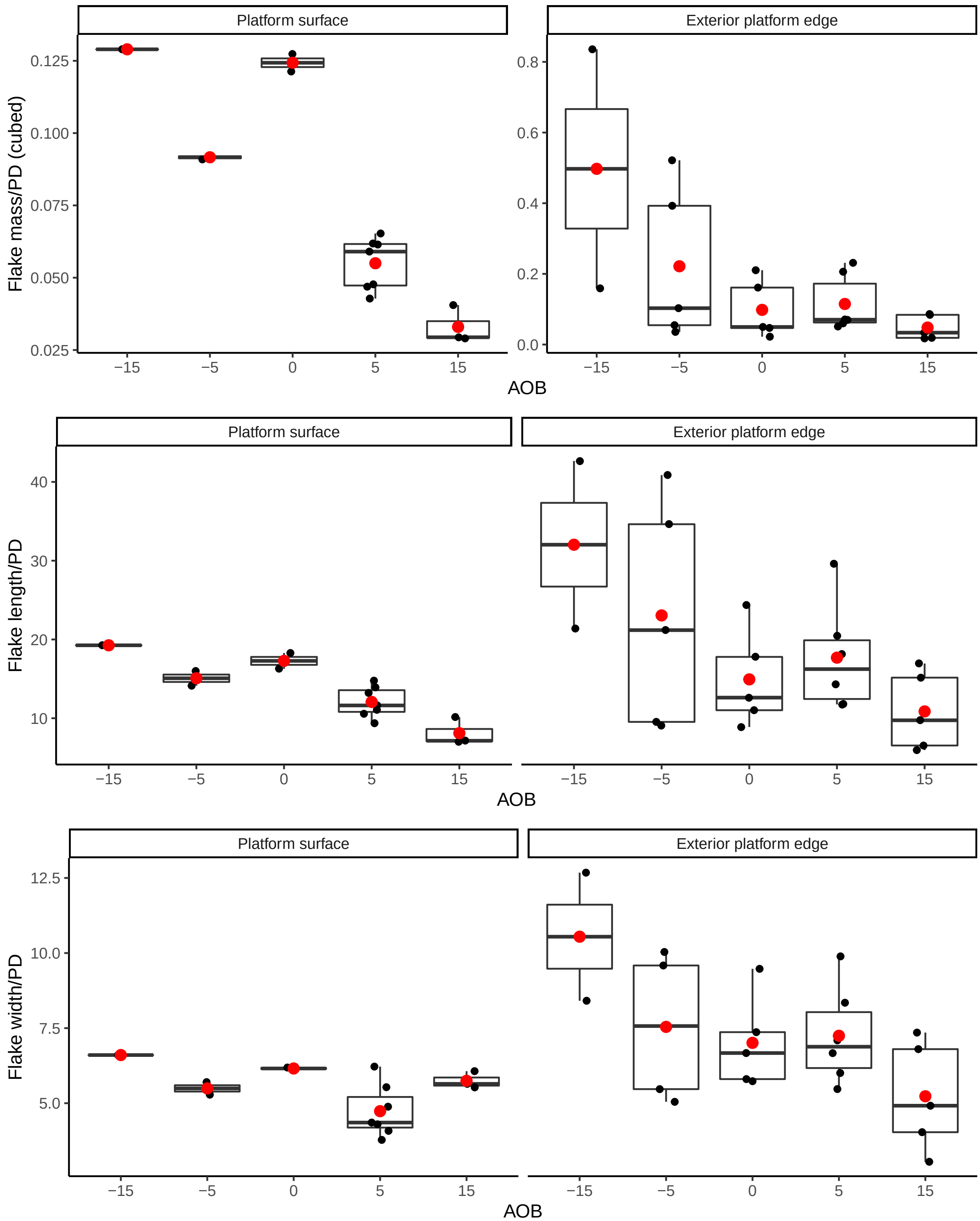

Fig.5 Flake weight relative to platform depth cubed by angle of blow (EPA = 65, copper hammer). Note that the means of weight/platform depth cubed between edge-struck and platform-struck are not significantly different, except in the case of AOB = 5.

Table 8 Mean values and sample size (N) of various dimension ratios by shape and size of the hammer (EPA = 65, AOB = 0, steel hammers). The first three entries of the table refer to the hammers with rounded tips.

Hammer end	Count	Len/Wid	Len/Thick	Wid/Thick	Len/PD	Wid/PD	Thick/PD	Weight/PD (cube)
3.2 mm	3	1.59	16.50	9.52	10.51	6.63	0.74	0.08
6.47 mm	3	1.32	11.16	8.05	9.37	7.02	0.92	0.08
9.51 mm	3	1.54	15.18	8.56	8.68	6.29	0.84	0.06
FLAT	2	1.32	15.81	10.87	14.57	10.36	0.98	0.18
EDGE	2	1.96	14.88	7.58	12.81	6.36	0.84	0.10

5 Leader et al. (2017)

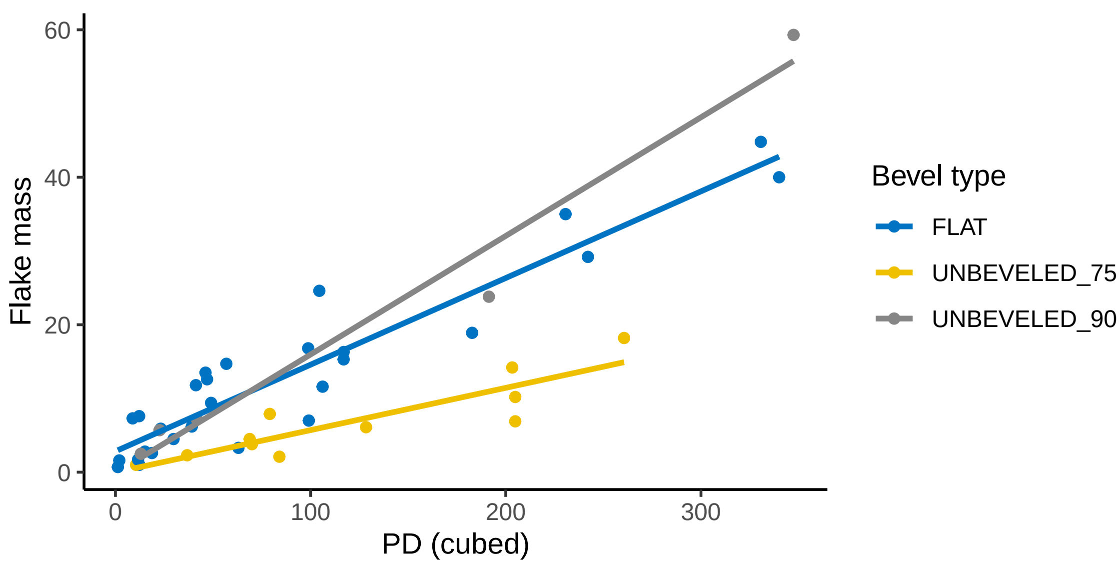

Fig.3 Scatter plot of flake weight and platform depth cubed for combined sample of flat-beveled flakes and unbeveled flakes produced with EPA of 75 and 90. In the bevel field, GRINDER represents concave bevel, SANDER represents flat bevel, and NONE represents either no bevel or lateral bevel.

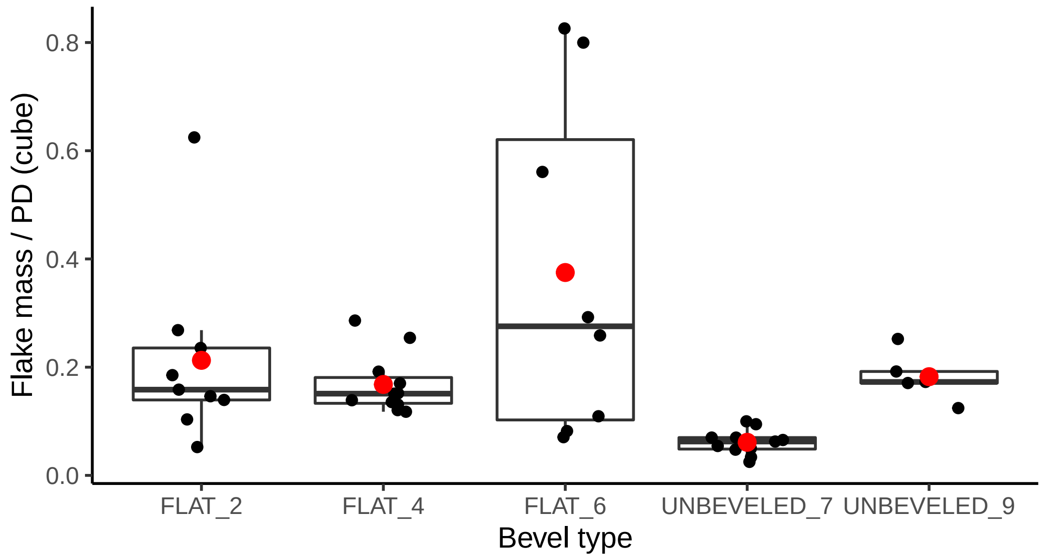

Fig.4 Boxplot of the ratio of flake weight to platform depth cubed for flat-beveled flakes compared with unbeveled flakes with EPA of 75 and 90.

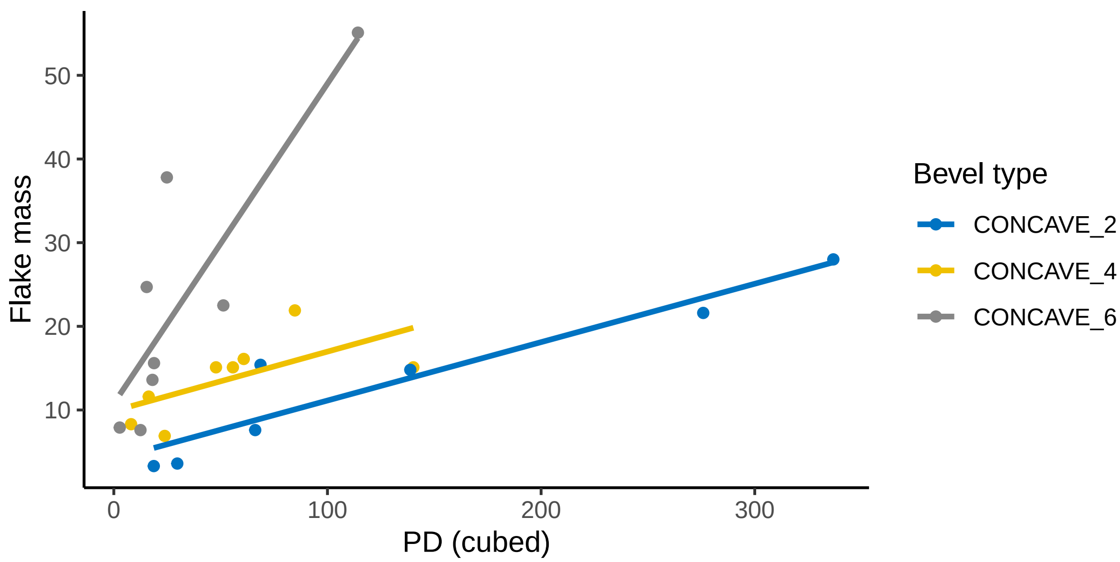

Fig.5 Scatter plot of flake weight and platform depth cubed for combined sample of concave-beveled flakes and unbeveled flakes produced with EPA of 75 and 90.

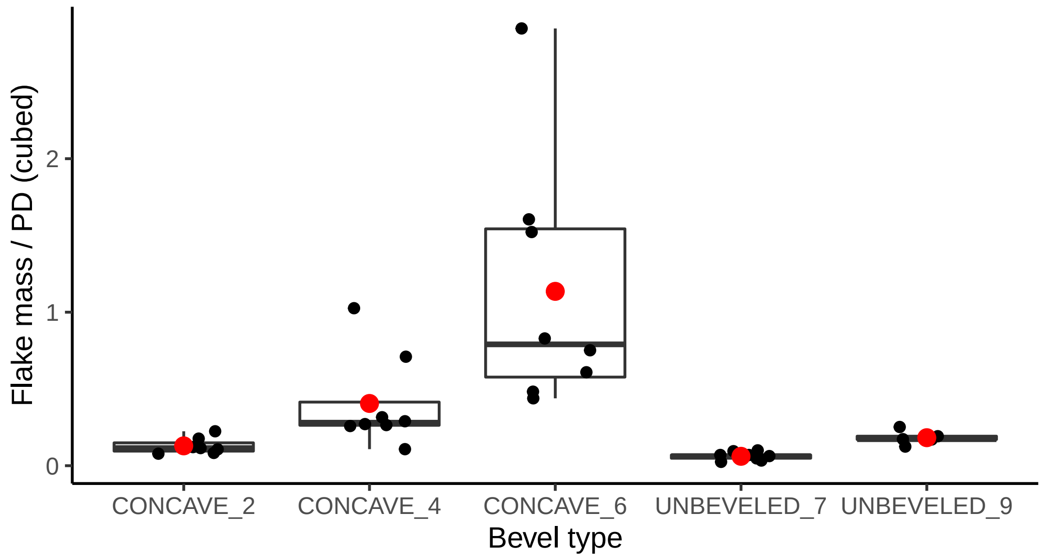

Fig.6 Box plots of the ratio of flake weight to platform depth cubed for concave-beveled flakes compared with unbeveled flakes with EPA of 75 and 90.

Table 1 Basic descriptive statistics and tests among different bevel classes for the ratios of flake weight to both platform depth and initial platform depth.

Bevel type	N	Flake mass / PD (cube)	Flake mass / Initial PD (cubed)
CONCAVE_2	7	0.129	0.039
CONCAVE_4	8	0.405	0.032
CONCAVE_6	8	1.136	0.030
FLAT_2	9	0.213	0.064
FLAT_4	6	0.178	0.033
FLAT_6	3	0.481	0.003
UNBEVELED_75	11	0.061	0.061
UNBEVELED_90	5	0.182	0.182

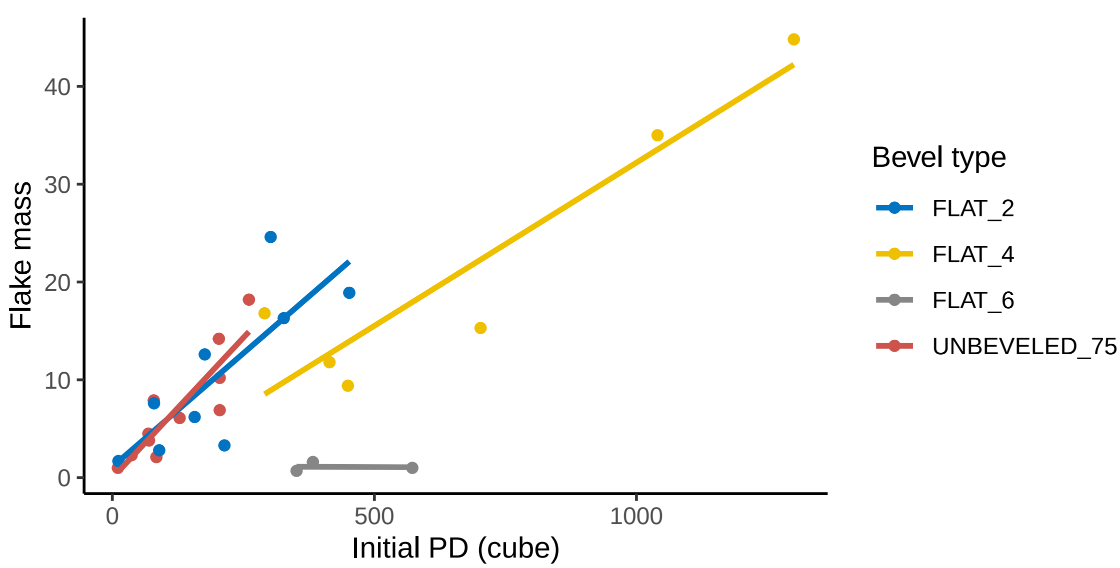

Fig.8 Scatter plot of flake weight and initial platform depth cubed for flat-beveled flakes of different bevel depths and unbeveled flakes produced with EPA = 75.

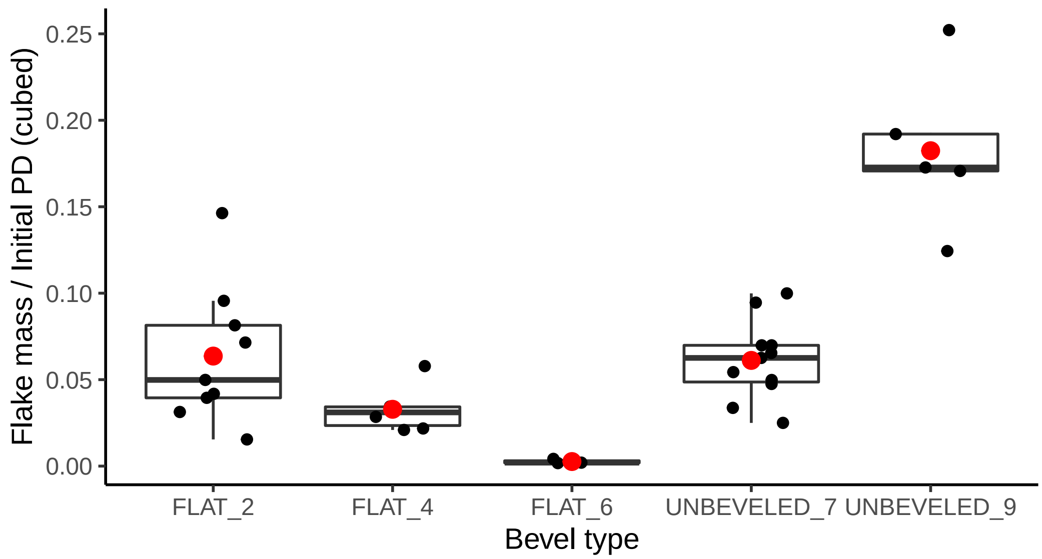

Fig.9 Boxplot of the ratio of flake weight to initial platform depth cubed for flat-beveled flakes compared with unbeveled flakes, EPA = 75 and 90.

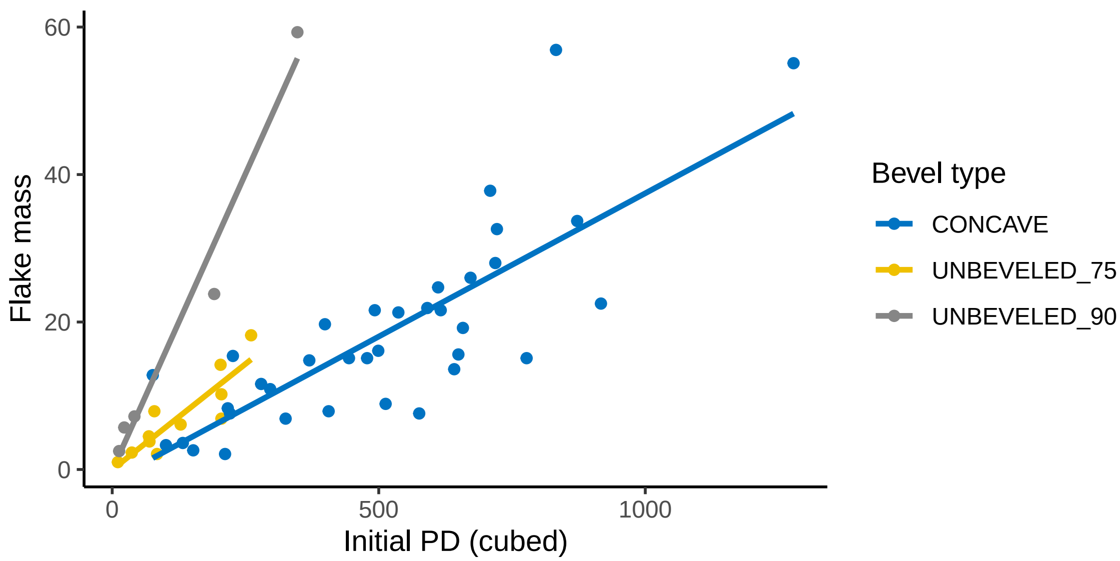

Fig.10 Scatter plot of flake weight and initial platform depth cubed for concave-beveled flakes of different bevel depths and unbeveled flakes produced with EPA = 75 and 90.

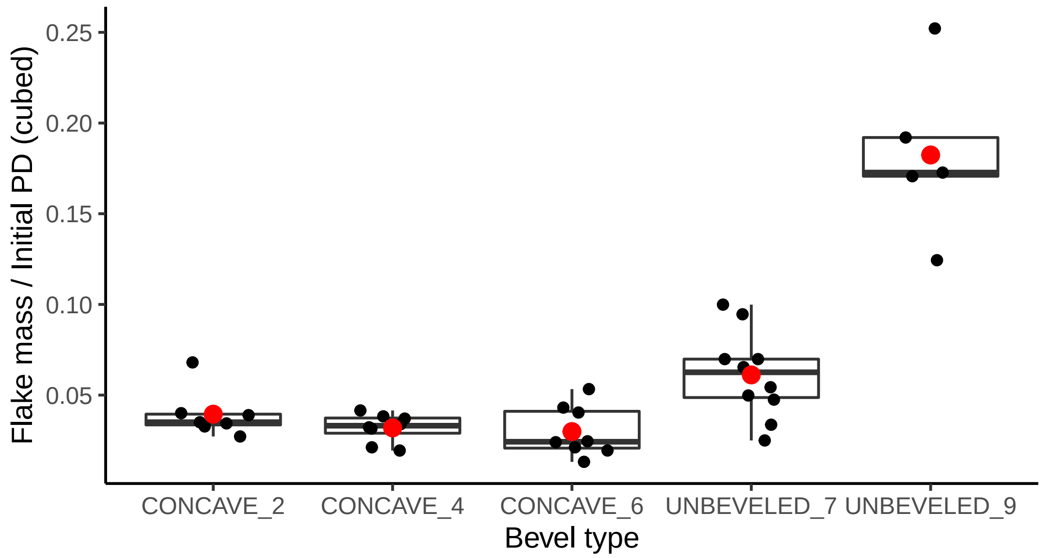

Fig.11 Boxplot of the ratio of flake weight to initial platform depth cubed for concave-beveled flakes compared with unbeveled flakes, with EPA = 75 and 90.

Table 3 Averages of bevel width, G2 refers to the 2mm bevel, G4 refers to the 4mm bevel, G4-8 refers to the narrow 4mm bevel, G4-30 refers to the wide 4mm bevel, G6 refers to the 6mm bevel.

Bevel type	N	Bevel width
G2	7	13.90
G4	8	18.32
G4-30	6	27.11
G4-8	7	7.72
G6	8	20.61

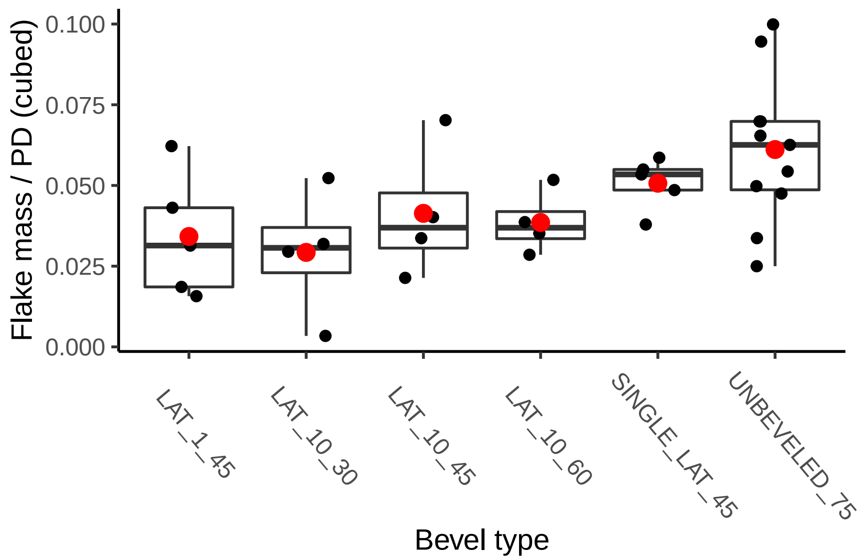

Fig.12 Boxplot of the ratio of flake weight to platform depth cubed for various classes of laterally-beveled flakes compared with unbeveled flakes with EPA = 75.

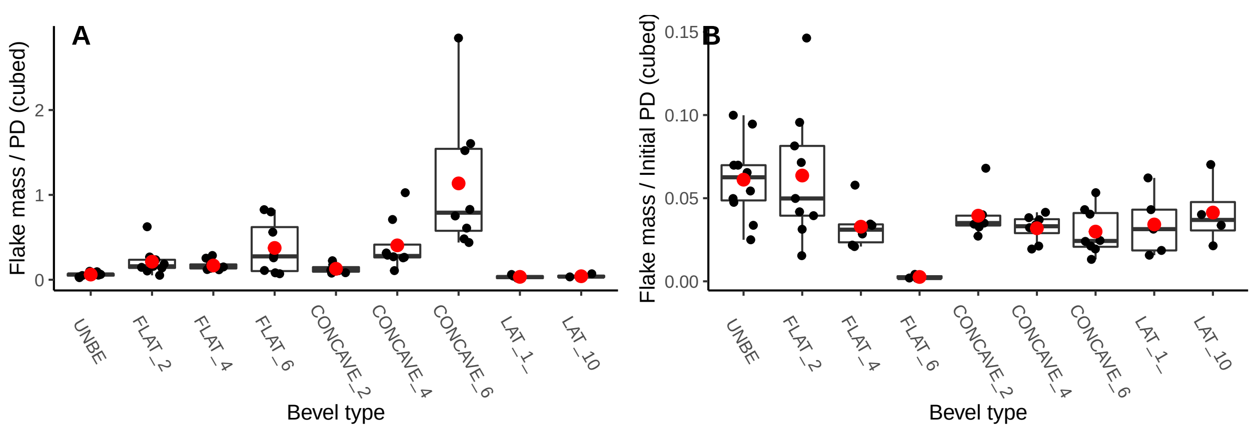

Fig.13 Boxplots showing ratios of (A) flake weight to platform depth and (B) flake weight to initial platform depth for various classes of bevels.

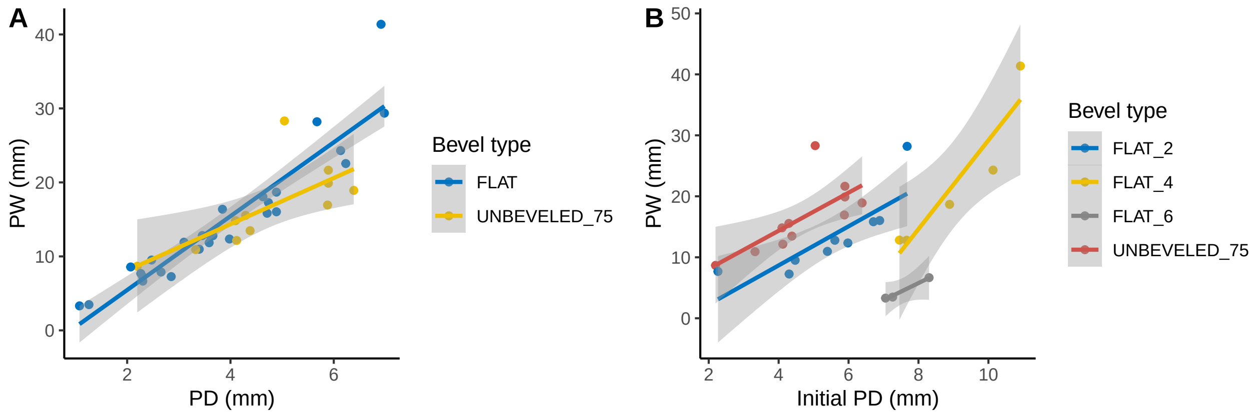

Fig.14 Scatter plots showing (A) platform width to platform depth for all bevel depths of flat-beveled flakes, (B) platform width vs. initial platform depth for each bevel depth of flat- beveled flakes.

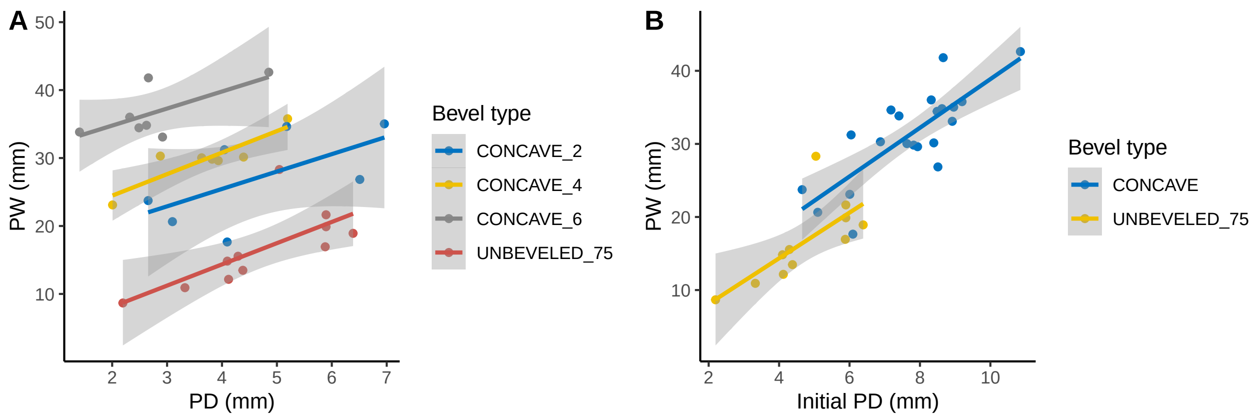

Fig.15 Scatter plots showing (A) platform width to platform depth for each bevel depth of concave-beveled flakes, (B) platform width vs. initial platform depth for all bevel depths of concave-beveled flakes.

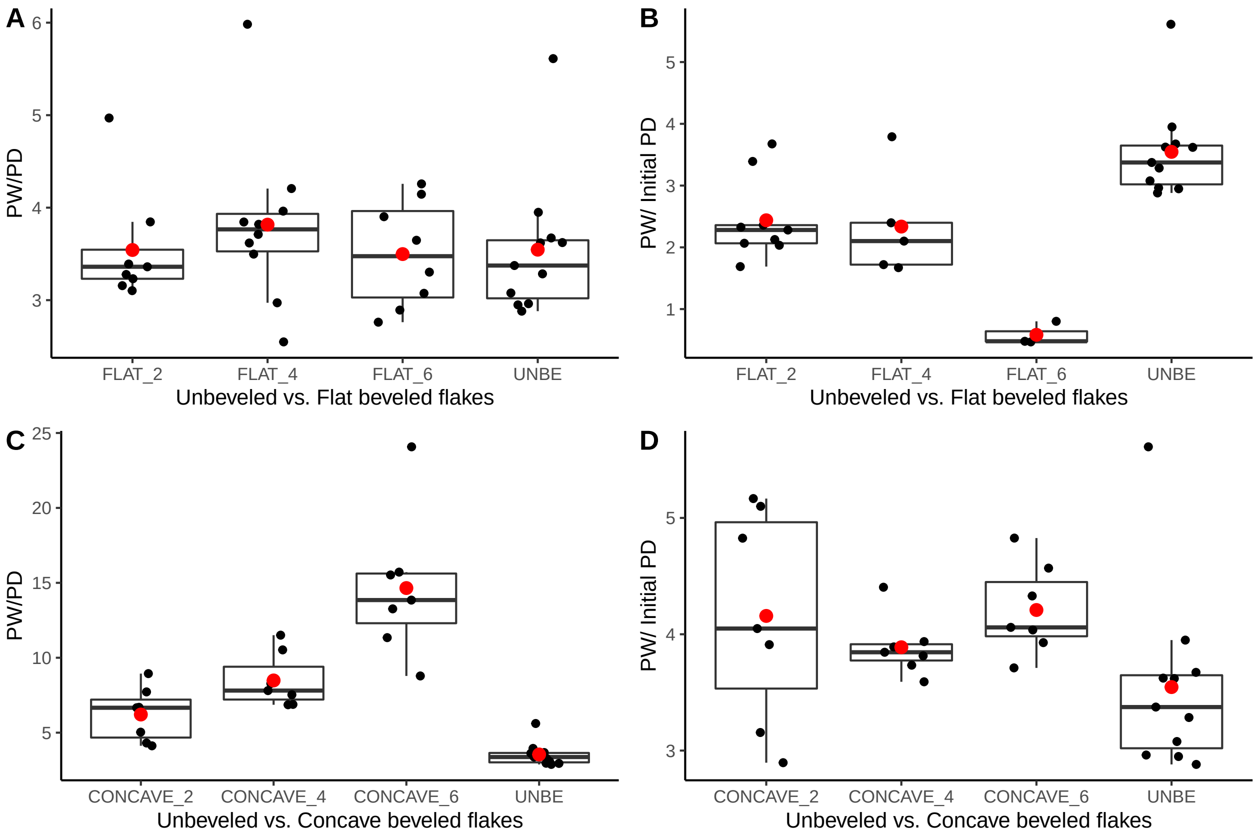

Fig.16 Boxplots of ratios of platform width to both platform depth and initial platform depth. (A) Platform width to platform depth, flat-beveled flakes; (B) Platform width to initial platform depth, flat-beveled flakes; (C) Platform width to platform depth, concave-beveled flakes; (D) Platform width to initial platform depth, concave-beveled flakes.

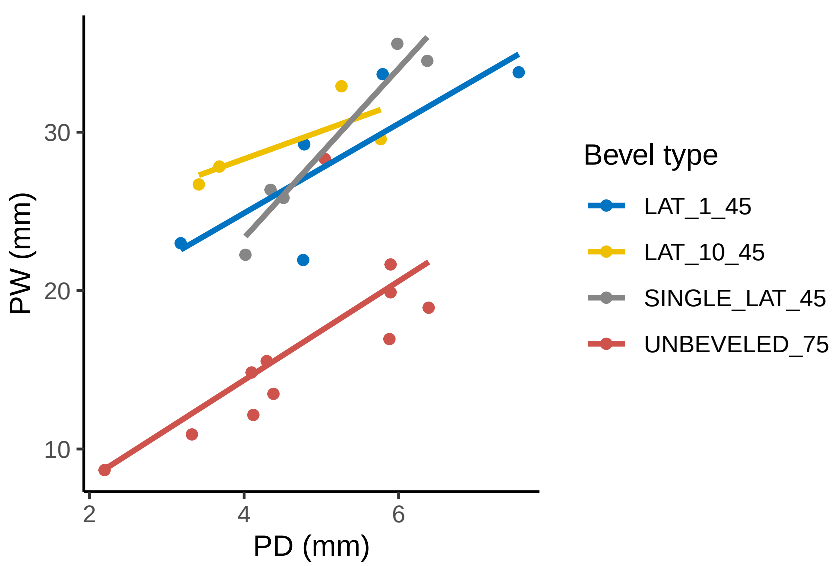

Fig.17 Relationship between platform width and platform depth for unbeveled cores, laterally-beveled cores with 1 mm and 10 mm platform surface, and cores with single lateral bevels. All bevel angles at 45° relative to the platform surface.

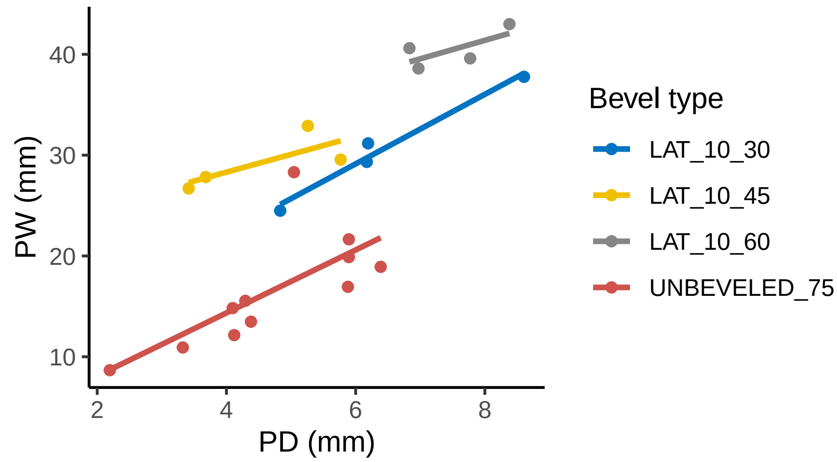

Fig.18 Relationship between platform width and platform depth for unbeveled cores and laterally-beveled cores with bevel angles at 30°, 45°, and 60° relative to platform surface. All platform surfaces of the beveled cores have a width of 10 mm.

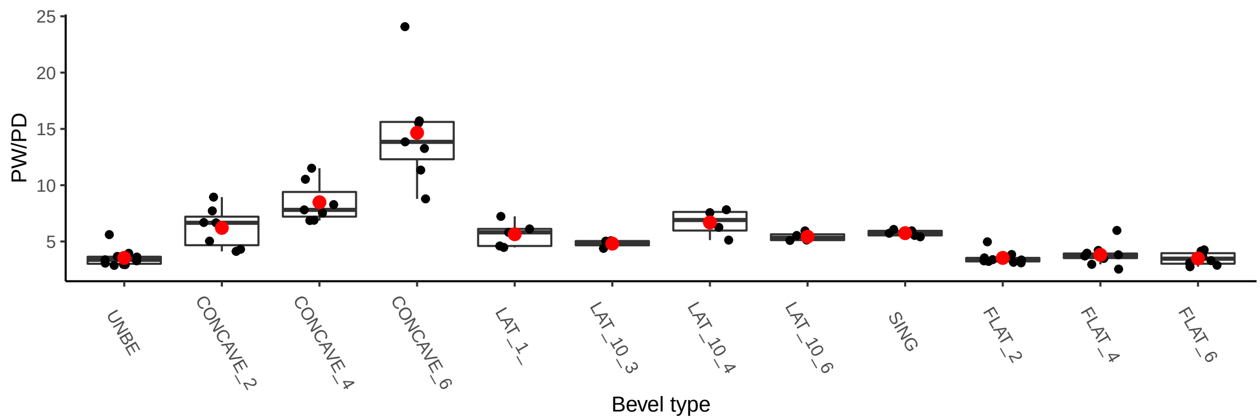

Fig.19 Box plots of ratio of platform width to platform depth for all of major bevel classes described above.

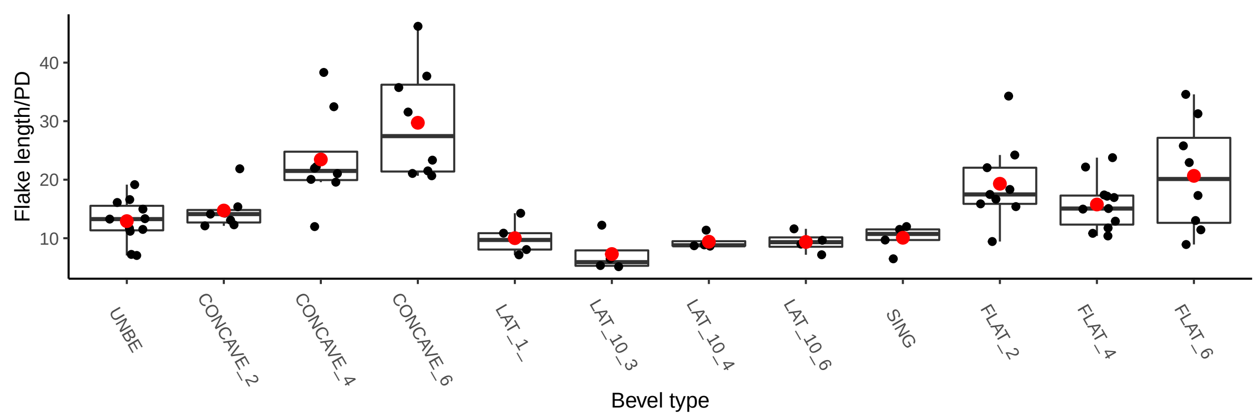

Fig.21 Box plots of ratio of flake length to platform depth for all of major bevel classes described above.

6 Dogandžić et al. (2020)

Table 1 Sample size by raw material and by EPA.

EPA	Glass	Baslt	Flint	Obsidian
65	4	5	5	5
75	4	7	6	6
85	3	4	4	4

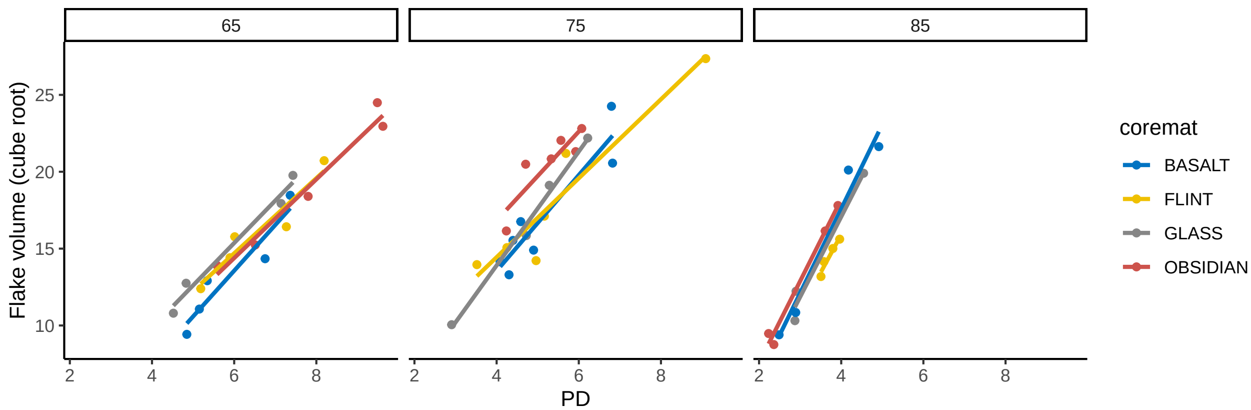

Fig.3 Volume (cube root) as a function of platform depth for each EPA group, by raw material.

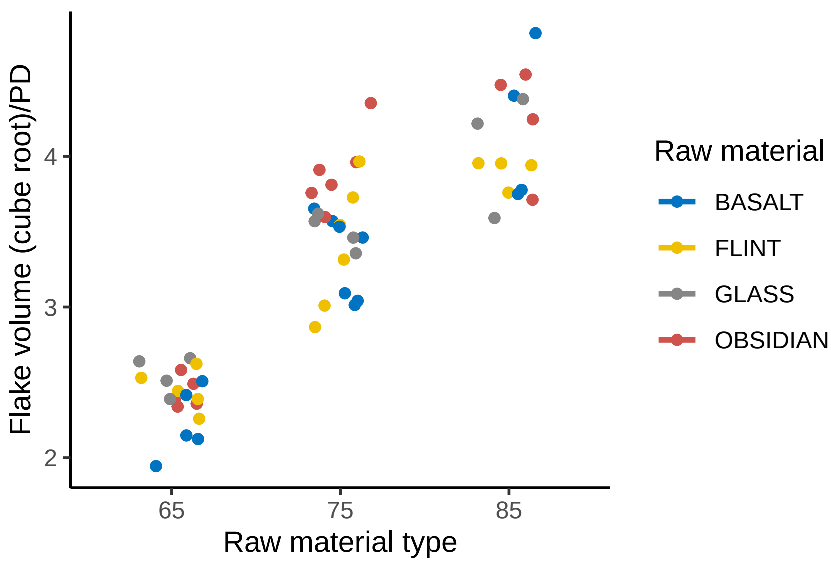

Fig.4 Dotplot showing the effect of EPA on flake volume (cube root of volume is standardized by platform depth) for different raw materials.

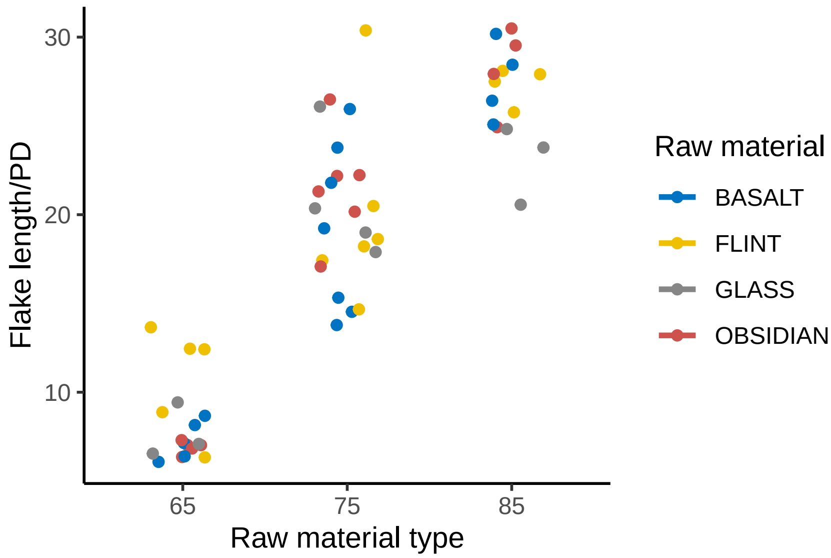

Fig.6 Dotplot showing the effect of EPA on flake length (standardized by platform depth) for different raw materials.

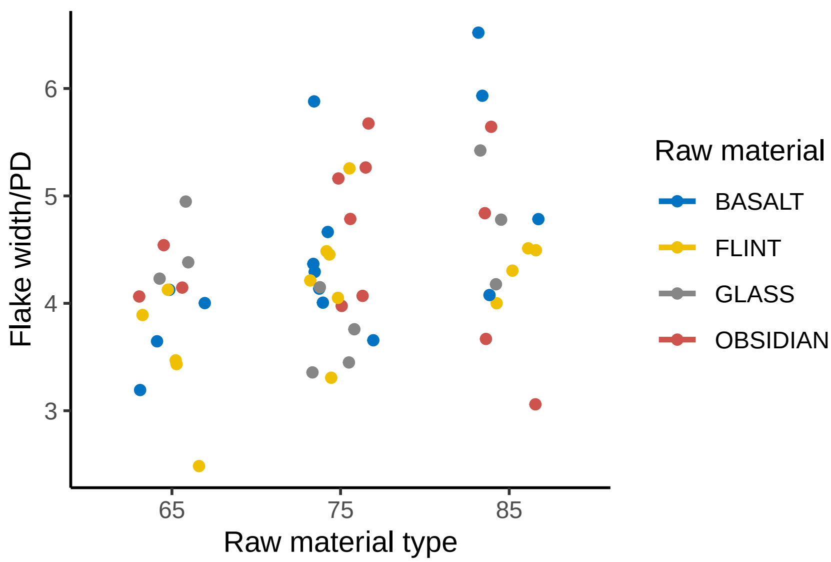

Fig.8 Dotplot showing the effect of EPA on flake width (standardized by platform depth) for different raw materials.

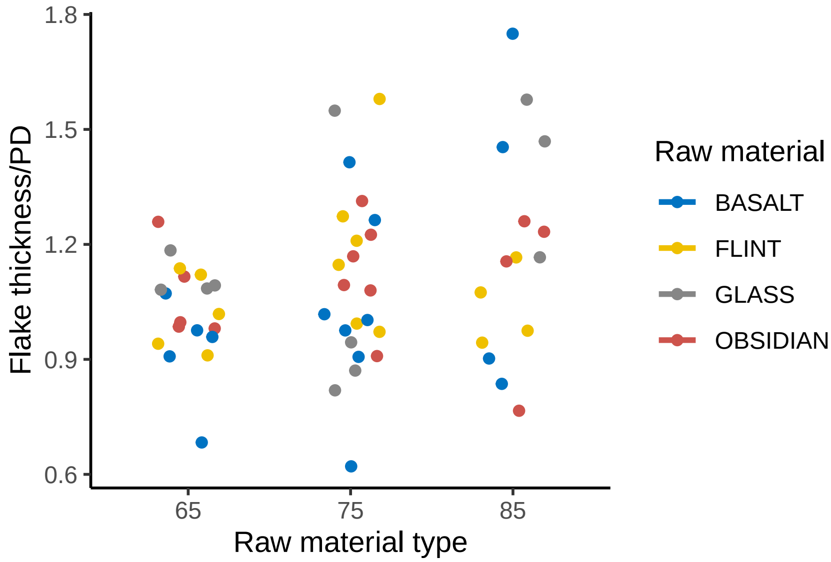

Fig.10 Dotplot showing the effect of EPA on flake thickness (standardized by platform depth) for different raw materials.

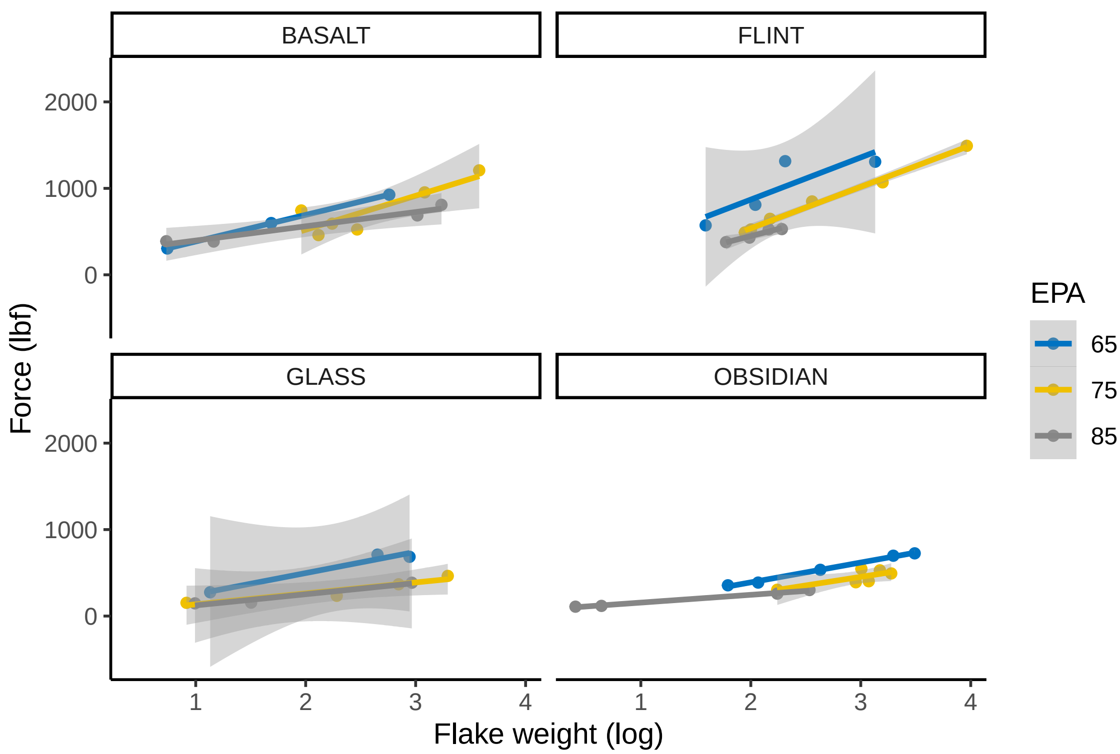

Fig.12 Relationship of force required to remove flakes by weight (log transformed) for different raw materials and varying EPAs.